Indian Journal of Engineering & Materials Sciences
Vol. 27, April 2020, pp. 277-287

Growth kinetics of Fe_2B layers formed on the AISI 4150 steel by different approaches

Jorge Zuno-Silva[a] , Mourad Keddam[b] , Martin Ortiz-Domínguez[a] , Milton Elias- Espinosa[c], Alberto Arenas-Flores[d] , Felipe Cervantes-Sodi[e] , José Angel Reyes-Retana[c,e]

[a]Autonomous University of Hidalgo State, Escuela Superior de Ciudad Sahagún-Mechanical Engineering, Carretera Cd. Sahagún-O tumba s/n, Zona Industrial CP. 43990, Hidalgo, México

[b] Laboratory of Materials Technology, Faculty of Mechanical Engineering and Process Engineering, USTHB, B.P. No. 32, 16111 El-Alia, Bab-Ezzouar, Algiers, Algeria.

[c] Monterrey Institute of Technology and Higher Education-ITESM Campus Santa Fe, Av. Carlos Lazo No. 100, Del. Álvaro Obregón, CP. 01389, México City, México.

[d] Materials and Metallurgy Research Center, Autonomous University of Hidalgo State, Ciudad Universitaria Pachuca-Tulancingo km. 4.5, Pachuca, Hidalgo, México.

[e] Ibero-American University of Mexico City, Department of Physics and Mathematics, Prolongación Paseo de la Reforma 880, Lomas de Santa Fe, CP. 01219, México City, México.

Received: 29 August 2017 ; Accepted:11 March 2020

In the present work, the AISI 4150 steel has been pack-borided in the temperature range of 1123-1273 K for a treatment time of 2 to 8 h. The mixture of powders containing 20% B_4C, 10% KBF_4 and 70% SiC has been used for producing a single boride layer (Fe_2B) at the surface of AISI 4150 steel. The presence of Fe_2B phase has been confirmed by XRD analysis. The SEM observations have been done to investigate the morphology of boride layers and measure their thicknesses. The cohesion of boride layers has been evaluated by using the Daimler-Benz Rockwell-C indentation technique. The borided sample at 1173 K for 8 h has shown a best cohesion of boride layer to the substrate in comparison to the sample treated at 1173 K during 2 h. Kinetically, different approaches have been used to estimate the boron diffusion coefficients in the Fe_2B layers and to predict the value of Fe_2B layer thickness obtained at 1253 K for a treatment time of 2.5 h. The estimated values of activation energies for boron diffusion in AISI 4150 steel have been in the range of 193.45 to 199.74 kJ mol^{-1}. These values of activation energies have been depended on the diffusion models used. In addition, a good agreement has been observed between the experimental value of Fe_2B layer thickness obtained at 1253 K for 2.5 h with the predicted values from these different diffusion models.

Keywords: Incubation time, Diffusion model, Activation energy, Growth kinetics, Integral method

1 Introduction

The boriding treatment is a thermochemical process in which boron atoms are diffused into the surface of steel parts resulting in the formation of a wear resistant boride layer[1]. The boriding process provides excellent surface properties such as high hardness, wear, corrosion and oxidation resistance[2,3]. The boriding treatment requires temperatures ranging from 800 to 1050 °C with a treatment time between 0.5 and 12 h. In case of ferrous alloys, the boride layer may be either a single phase layer (Fe_2B) or a double phase layer (FeB and Fe_2B) depending on the boron activity in the boriding agent and also on the boriding parameters (time and temperature). For tribological applications, a single boride layer (Fe_2B) is suitable since it is less brittle and tougher than FeB [4,5].

The boriding process can be carried out with boron in different states such as powder [6-10], paste[11,12], liquid [13-15], gas [16-18], plasma[19-21]. Amongst all these boriding techniques, pack -boriding is the most attractive because of its economic advantage, and it is widely used in the industry [22,23].

From a kinetic viewpoint, different approaches about the modeling of the growth of Fe_2B layers on different substrates[24-38] are available in the literature data. Certain models considered the occurrence of boride incubation times during the formation of Fe_2B layers. For example, Elias-Espinosa *et al.*[24] have developed a kinetic model based on solving the mass balance Eq. at the (Fe_2B/ substrate) interface by

*Corresponding author (E-mail: keddam@yahoo.fr)

introducing a non dimensional kinetic parameter with the presence of a constant boride incubation time independent of the boriding temperature. Similarly, Ortiz-Domínguez *et al.*[25] have investigated the growth kinetics of Fe_2B layers formed on a gray cast iron via powder-pack boriding by solving the mass balance Eq. at the (Fe_2B/substrate) interface and assuming a parabolic growth law for Fe_2B. In addition, Kouba *et al.*[30] have used a sharp interface approach to solve numerically the growth kinetics of Fe_2B layers on Armco iron by considering simultaneously the diffusion of boron atoms into the Fe_2B phase and the displacement of the (Fe_2B/substrate) interface with the treatment time. In their model, the diffusivity of boron in the austenite was considered and the boron flux at the surface before the formation of Fe_2B was adjusted in order to experimentally reproduce the boride incubation time for Fe_2B at a given boriding temperature. A recent approach based on the integral method was developed to be applied to the growth kinetics of Fe_2B layers on AISI 12L14 steel[29]. In this approach, an analytic solution was obtained from a system formed by differential algebraic Eq.s (DAE) to get a simple expression relating the diffusion coefficient of boron in Fe_2B to the square of parabolic growth constant at the (Fe_2B/substrate) interface.

In the present study, a recent diffusion model based on the integral method was proposed to estimate the boron diffusion coefficients in the Fe_2B layers on the AISI 5140 steel's substrate in the temperature range of 1123–1273 K. It is noted that this alternative model was inspired from the reference works[39,40]. This kinetic approach was already used to investigate the growth kinetics of ε and γ' iron nitrides formed on the plasma nitrided pure iron.

The aim of the present work was to investigate the boriding kinetics of AISI 4150 steel and the cohesion of Fe_2B layers on the surface of AISI 4150 steel. Till now, there is no kinetic study regarding the pack-boriding of AISI 4150 steel. For this reason, different diffusion models were used to estimate the boron diffusion coefficients in Fe_2B in the temperature range of 1123-1273 K. Basing on our experimental results, the values of activation energy for boron diffusion in the AISI 4150 steel were estimated from different approaches and compared with the literature data.

2 The Kinetic Model Based on the Integral Method

The diffusion model is concerned with the growth kinetics of Fe_2B layer on a saturated substrate with boron atoms. The boron concentration– profile through the Fe_2B layer is displayed in Fig. 1. The growth kinetics of the Fe_2B layer during a diffusion-controlled phase transformation in the Fe-B system is analyzed by taking into account the displacement of the (Fe_2B/substrate) interface.

The difference of the arrival flux of interstitial boron atoms to Fe_2B phase and the departure flux of the boron atoms from this phase to the matrix leads to the displacement of the (Fe_2B/substrate) interface. After a time surpassing the boride incubation time $t_0^{Fe_2B}(T)$, the Fe_2B layer begins to form and becomes continuous and more compact after a prolonged treatment time. $C_{up}^{Fe_2B}$ denotes the upper limit of boron content in Fe_2B (=9 wt.%), $C_{low}^{Fe_2B}$ is the lower limit of boron content in Fe_2B (=8.83 wt.%) and the point x(t)=u represents the Fe_2B layer thickness. From a thermodynamic point of view, the Fe_2B phase exhibits a narrow composition range (of about 1 at. %) as stated by the authors [41]. The term C_{ads} is the adsorbed boron concentration in the boride layer during the boriding treatment [42]. C_0 is the boron solubility in the matrix which is very low (≈ 0 wt.%)[43-46]. The following assumptions are considered during the establishment of diffusion model [29]

- The growth kinetics is governed by the phenomenon of boron diffusion.
- The Fe_2B phase nucleates after a certain incubation period.

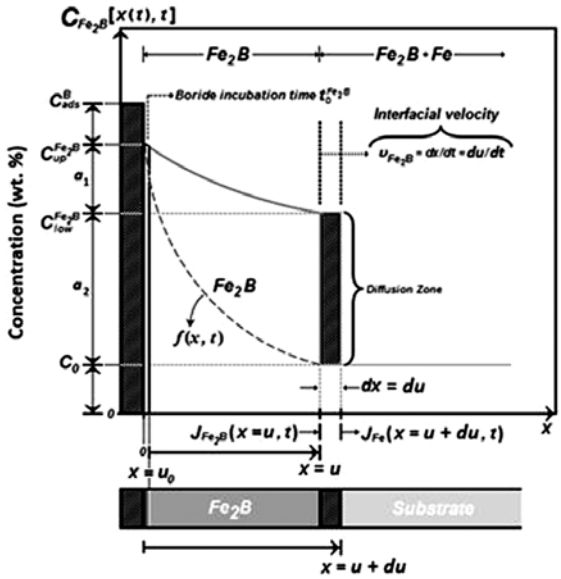

Fig. 1 — A schematic representation of boron concentration profile through the Fe_2B layer

- Boron concentrations do not vary during the boriding treatment.
- The boride layer is thin in comparison with the sample thickness.
- Planar morphology is assumed for the (Fe_2B/substrate) interface.

The initial and boundary conditions for the diffusion problem are represented as:

$$t = 0, x > 0, \text{ with } C_{Fe_2B}[x(t), t = 0] = C_0 \approx 0 \text{ wt.\%} \quad \ldots (1)$$

Boundary conditions:

$$C_{Fe_2B}[x(t = t_0^{Fe_2B}) = 0, t = t_0] = C_{up}^{Fe_2B} \text{ for } C_{ads} > 8.83\text{wt.\%} \quad \ldots (2)$$

$$C_{Fe_2B}[x(t = t) = u(t), t = t] = C_{low}^{Fe_2B} \text{ for } C_{ads} < 8.83 \text{ wt.\%} \quad \ldots (3)$$

The boron concentration profile through the Fe_2B layer is described by the Second Fick's law as follows:

$$D_{Fe_2B}\frac{\partial^2 C_{Fe_2B}[x,t]}{\partial x^2} = \frac{\partial C_{Fe_2B}[x,t]}{\partial t} \quad \ldots (4)$$

where the boron diffusion coefficient in Fe_2B depends upon the boriding temperature. The boron-concentration profile along the Fe_2B layer is described by the Goodman's method[47] as follows:

$$C_{Fe_2B}[x,t] = C_{low}^{Fe_2B} + a(t)(u(t) - x) + b(t)(u(t) - x)^2 \text{ for } 0 \le x \le u \quad \ldots (5)$$

The three time-dependent unknowns a(t), b(t) and u(t) are subjected to the boundary conditions given by Eqs (2) and (3). It is noted that the two parameters a(t) and b(t) should be positive because of a decreasing nature of the boron–concentration profile. By applying the boundary condition on the surface, Eq. (6) was obtained:

$$a(t)u(t) + b(t)u(t)^2 = (C_{up}^{Fe_2B} - C_{low}^{Fe_2B}) \quad \ldots (6)$$

By integrating the second Fick's law between 0 and u(t) and applying the Leibniz rule, the ordinary differential Equation (ODE) given by Eq. (7) was deduced :

$$\frac{u(t)^2}{2}\frac{da(t)}{dt} + a(t)u(t)\frac{du(t)}{dt} + \frac{u(t)^3}{3}\frac{db(t)}{dt} + b(t)u(t)^2\frac{du(t)}{dt} = 2D_{Fe_2B}b(t)u(t) \quad \ldots (7)$$

The mass balance Equation at the (Fe_2B/substrate) interface can be formulated by Eq. (8) as follows:

$$W\left.\frac{dx}{dt}\right|_{x=u} = -D_{Fe_2B}\left.\frac{\partial C_{Fe_2B}[x,t]}{\partial x}\right|_{x=u}$$

$$\text{with } W = [\frac{(C_{up}^{Fe_2B} - C_{low}^{Fe_2B})}{2} + (C_{low}^{Fe_2B} - C_0)] \quad \ldots (8)$$

At the (Fe_2B/substrate) interface, the boron concentration remains constant and Eq. (8) can be rewritten as:

$$W(-\frac{\left.\frac{\partial C_{Fe_2B}[x,t]}{\partial t}\right|_{x=u}}{\left.\frac{\partial C_{Fe_2B}[x,t]}{\partial x}\right|_{x=u}}) = -D_{Fe_2B}\left.\frac{\partial C_{Fe_2B}[x,t]}{\partial x}\right|_{x=u} \quad \ldots (9)$$

Substituting Eq. (4) into Eq. (9) and after derivation with respect to the diffusion distance x(t), Eq. (10) was obtained:

$$(C_{up}^{Fe_2B} + C_{low}^{Fe_2B})b(t) = a(t)^2 \quad \ldots (10)$$

Eqs (6), (7) and (10) constitute a set of differential algebraic Eq.s (DAE) in a(t), b(t) and u(t) subjected to the initial conditions taken from the experimental results. This resulting DAE system can be solved analytically. To determine the expression of boron diffusion coefficient in the Fe_2B layers, an analytic solution exists for this diffusion problem by setting:

$$u(t) = k[t - t_0^{Fe_2B}(T)]^{1/2} \quad \ldots (11)$$

where u(t) is the Fe_2B layer thickness, $t_0^{Fe_2B}(T)$ the associated boride incubation time and k the parabolic growth constant of the Fe_2B layer. It is noticed that the use of Eq. (11) is acceptable from a practical point of view since it has been observed in many experiments. After substitution of Eq. (11) into the DAE system and derivation, the expression of boron diffusion coefficient was obtained as follows:

$$D_{Fe_2B} = k^2[(\frac{1}{16})(\frac{C_{up}^{Fe_2B} + C_{low}^{Fe_2B}}{C_{up}^{Fe_2B} - C_{low}^{Fe_2B}})(1 + \sqrt{1 + 4(\frac{C_{up}^{Fe_2B} - C_{low}^{Fe_2B}}{C_{up}^{Fe_2B} + C_{low}^{Fe_2B}})}) + (\frac{1}{12})] \quad \ldots (12)$$

along with the expressions of a(t) and b(t) given by

Eqs (13) and (14):

$$a(t)=\frac{(C_{up}^{Fe_2B}+C_{low}^{Fe_2B})[-1+\sqrt{1+4(\frac{C_{up}^{Fe_2B}-C_{low}^{Fe_2B}}{C_{up}^{Fe_2B}+C_{low}^{Fe_2B}})}]}{2k[t-t_0^{Fe_2B}(T)]^{1/2}} \quad \ldots (13)$$

$$b(t)=\frac{(C_{up}^{Fe_2B}+C_{low}^{Fe_2B})[2+4(\frac{C_{up}^{Fe_2B}-C_{low}^{Fe_2B}}{C_{up}^{Fe_2B}+C_{low}^{Fe_2B}})-2\sqrt{1+4(\frac{C_{up}^{Fe_2B}-C_{low}^{Fe_2B}}{C_{up}^{Fe_2B}+C_{low}^{Fe_2B}})}]}{4k^2[t-t_0^{Fe_2B}(T)]} \quad \ldots (14)$$

It is seen that the parameters a(t) et b(t) are found to be positive.

3 Experimental Details

3.1 The material and the boriding process

The AISI 4150 steel was used as the substrate in this study. It had a nominal chemical composition of 0.48–0.53% C, 0.20–0.35% Si, 0.75–1.00% Mn, 0.80–1.10% Cr, 0.15–0.25% Mo, 0.035 % P and 0.040% S. The samples to be treated were cut to dimensions of 10 mm×10 mm×10 mm. Before the boriding treatment, they were polished, ultrasonically cleaned in an alcohol solution and deionized water for 15 min at room temperature, dried and stored under clean-room conditions. The samples were embedded in a closed, cylindrical case in contact with a mixture of powders composed of 20% B_4C as the donor, 10% KBF_4 as an activator, and 70% SiC as the diluent. The powder-pack boriding process was carried out in a conventional furnace under a pure argon atmosphere in the temperature range of 1123-1273 K. Four treatment times (2, 4, 6 and 8 h) were chosen for each temperature. Once the boriding treatment was finished, the container was removed from the furnace and slowly cooled to room temperature.

3.2 Experimental techniques

The borided and etched samples were cross-sectioned for microstructural investigations using a LECO VC-50 cutting precision machine. The cross-sections of formed boride layers were observed by SEM (JEOL JSM 6300 LV) and by optical microscope (Olympus GX51) in a clear field. A kinetic investigation was made by measuring automatically the boride layer thickness by means of MSQ PLUS *software*. To ensure the reproducibility of the measured layers, seventy measurements were collected in different sections of the borided samples to estimate the Fe_2B layer thickness; defined as an average value of the long boride teeth [48-51].

The phase formed on the surface of borided sample was identified by means of X-Ray Diffraction (XRD) equipment (Equinox 2000) using Co-K_α radiation at λ_{Co} = 0.179 nm. The Daimler-Benz Rockwell-C technique, using an indenter tester, was performed to get a qualitative information on the cohesive strength of the boride layers to the substrate. The well-known Rockwell-C indentation test is prescribed by the VDI 3198 norm, as a destructive quality test of coated compounds [52-55].

The principle of this method was given in the reference work[52]. A load of 1471 N was applied to cause coating damage adjacent to the boundary of the indentation. Three indentations were made for each borided sample to assess the cohesion test. The indentation craters were examined by SEM. During the cohesion test, a conical diamond indenter penetrated into the surface of an investigated layer, thus inducing massive plastic deformation to the substrate and fracture of the boride layer. The damage of the boride layer was compared with the cohesion strength quality maps HF1-HF6 displayed in Fig. 2.

In general, the cohesion strength HF1- HF4 is defined as sufficient cohesion, whereas HF5 and HF6 represent insufficient cohesion[52,53].

4 Results and Discussion

4.1 SEM observations and EDS analysis

Figure 3 shows the SEM micrographs of the cross-sections of borided steels at 1173 K during 2, 4, 6 and 8 h. It is seen that the needles of Fe_2B borides are visible exhibiting a tooth-shaped morphology for all boriding conditions. This peculiar morphology ensures a good adhesion to the substrate[56,57]. The thickness of Fe_2B layer increased when increasing the boriding temperature since the mobility of boron atoms into the substrate is accelerated by thermodiffusion. The value of Fe_2B layer thickness ranged from 43.53 ± 5.68 μm for 2 h to 98.45 ± 15.6 μm for 8 h at 1173 h.

The EDS analysis was done at the surface of borided sample and in the areas located at the

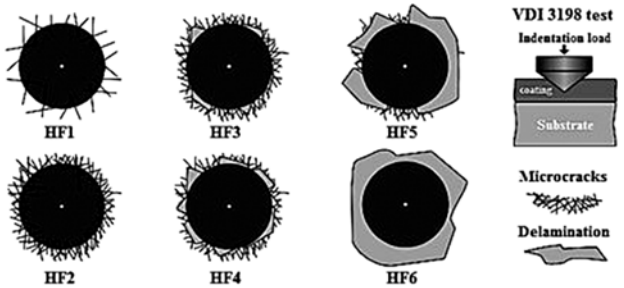

Fig. 2 — Principle of the VDI 3198 indentation test [53].

(Fe_2B/substrate) interface. The SEM micrographs

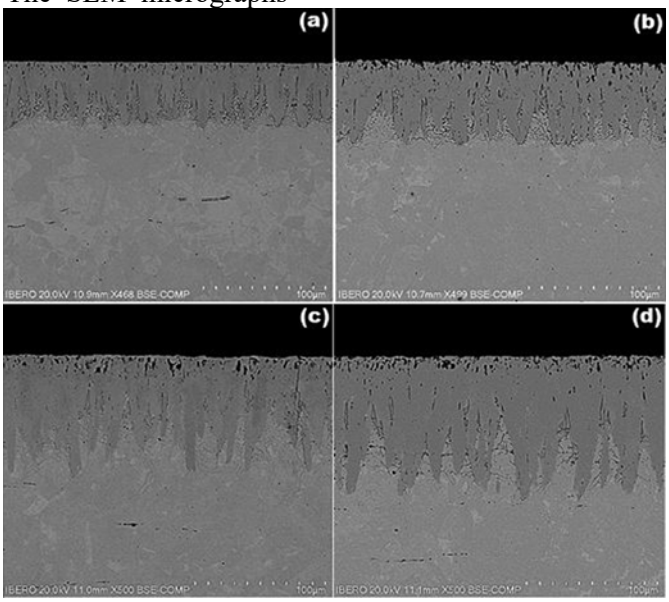

Fig. 3 — SEM micrographs of the cross-sections of AISI 4150 steels borided at 1173 K for increasing treatment times: (a) 2 h, (b) 4 h, (c) 6 h, and (d) 8 h.

displayed in Fig. 4 show the analyzed zones. Figure 4 (a) indicates the presence of Fe element together with other elements such as Mn, Cr and B. In fact, iron atoms combine with boron atoms to form the Fe_2B phase if the lower limit of boron concentration is reached in Fe_2B by a mechanism of nucleation and growth of Fe_2B crystals. Moreover, if we zoom in on the graph of the Fig. 4 (a), we can look at the B element is hard to be detected by EDS, because the energy that corresponds to the B element is 0.18 keV. This is an evidence that boron element is present at the surface of borided sample at 1173 K for 2 h. Figure 4(b) shows an EDS analysis with the presence of the following elements: Fe, C, Si, P, Mn, Mo and Cr. Carbon and Silicon are diffused towards the diffusion zone by forming together with boron, solid solutions like silicoborides ($FeSi_{0.4}B_{0.6}$ and Fe_5SiB_2) and boroncementite $Fe_3B_{0.67}C_{0.33}$ [41,58].

4.2 X-ray diffraction analysis

Figure 5 shows the XRD pattern obtained at the surface of borided AISI 4150 steel at a temperature of 1273 K for a treatment time of 8 h. The diffraction peaks are readily identified for the Fe_2B phase with the strongest peak belonging to the (002) crystallographic plane. The boride needles grow in the direction of minimum resistance [001] exhibiting a saw-tooth morphology [56]. In addition, no metallic borides were identified by XRD analysis in AISI 4150 steel.

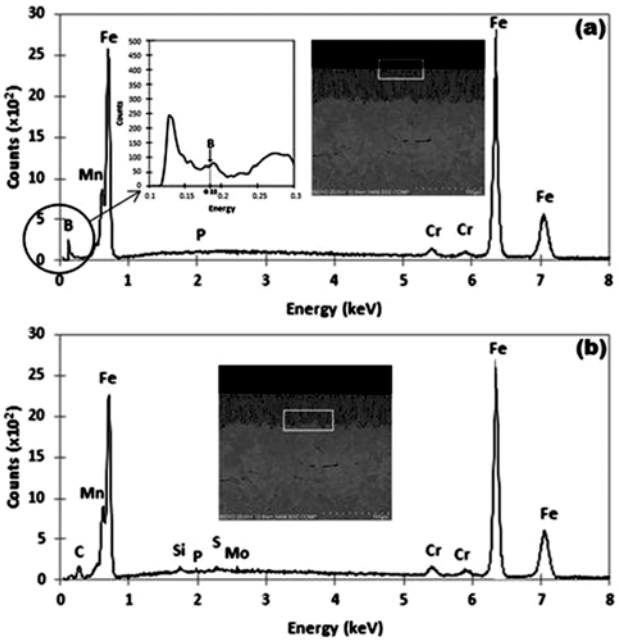

Fig. 4 — SEM micrographs with EDS analysis of the cross-sections of the borided AISI 4150 steel at 1173 K for 2 h a) EDS spectrum at the surface of borided sample, and (b) EDS spectrum at the (Fe_2B/substrate) interface.

4.3 Rockwell-C cohesion test

To determine the cohesion of the boride layers to the substrate, the cohesion tests were applied on the two pack-borided samples (at 1173 K for 2 h and 8 h). Figure 6 shows the SEM micrographs of the

indentation craters generated on the surfaces of two borided samples. Figure 6 (a) revealed an existence of radial cracks at the perimeter of indentation crater with delamination. The cohesion strength quality of boride layer obtained at 1173 K for 2 h was related to the H3 category.

Figure 6 (b) shows the presence of a small quantity of spots with flaking caused by delamination. The cohesion strength quality of boride layer, obtained at 1173 K during 8 h, was identified as HF2 category. It is seen that the two borided samples (at 1173 K for 2 h and 8 h) had sufficient cohesion. Nevertheless, the borided sample at 1173 K during 8 h showed a best cohesion since it had a thicker boride layer in comparison with the borided sample at 1173 K for 2 h. There are some cracks and delamination in the crater, but they did not look like it, because we did not zoom in on the crater. Moreover, the Daimler-Benz adhesion test is used as a destructive quality test for coating/substrate system. In this sense, the coatings at high temperature and treatment time present a good cohesion due to the interdiffusion phenomenon ensuring the continuity of metallic interface [24], as it can be seen in the Fig. 6 (b). These coatings are therefore less exposed to damage characterized by the separation of the interfaces. In this context, Ortiz-Dominguez *et al.*[25] showed also the occurence of cracks and delamination in the crater of the boride coating using the Daimler–Benz method.

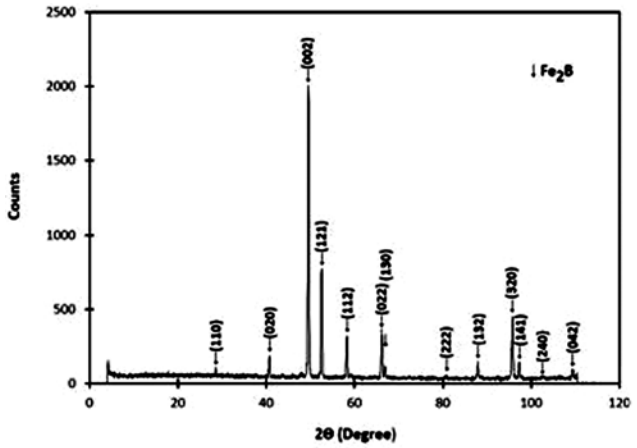

Fig. 5 — XRD pattern obtained at the surface of borided AISI 4150 steel at 1273 K for 8 h.

Kartal *et al.*[59] carried out a new electrochemical boriding method on AISI 1018 steel. They showed that was possible to form a single boride layer (Fe_2B) after the electrochemical boriding, for 15 min followed by the phase homogenization during 45 min. The Rockwell –C cohesion test on this treated sample had a very sufficient cohesion to the substrate consistent with the H1 category without cracks and delamination.

4.4 Estimation of activation energy for boron diffusion by different approaches

To estimate the value of activation energy for boron diffusion in AISI 4150 steel, it is necessary to have the kinetic data regarding the variation of square of Fe_2B layer thickness as a function of boriding time. Figure 7 describes the time dependence of square of Fe_2B layer thickness for increasing temperatures. Table 1 provides the experimental values of parabolic growth constants at the (Fe_2B/substrate) interface along with the corresponding boride incubation times deduced from Fig. 7. It is noticed that the boride incubation time is constant and do not change with the boriding temperature. The temperature dependence of the boron diffusion coefficient in Fe_2B is expressed by Eq. (15):

$$D_{Fe_2B} = D_0 \exp(-\frac{Q}{RT}) \qquad \ldots(15)$$

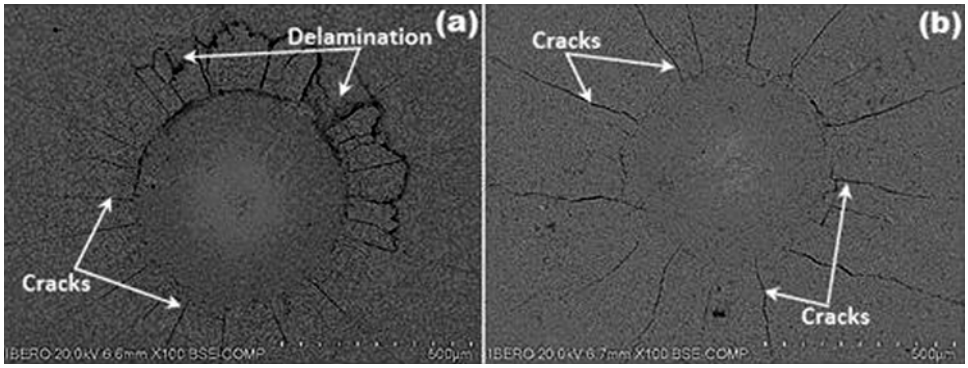

Fig. 6 — SEM micrographs showing indentation of VDI cohesion tests at the surfaces of borided AISI 4150 steels : (a) at 1173 K for 2 h and (b) at 1173 K for 8 h.

where D_0 is the diffusion coefficient of boron

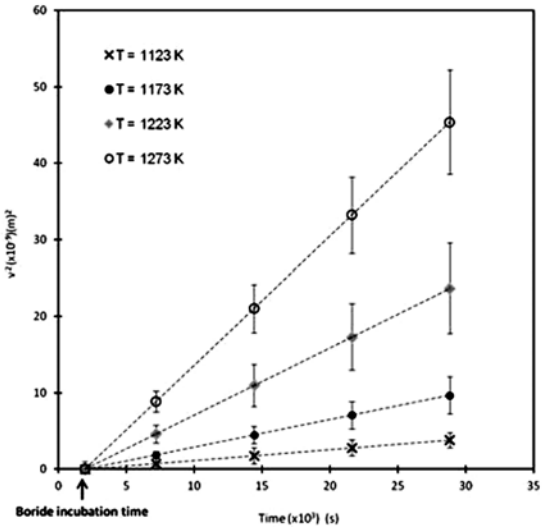

Fig. 7 — The square of Fe_2B layer thickness as a function of the boriding time.

Table 1 — Experimental values of parabolic growth constants at the (Fe_2B/substrate) interface along with the corresponding boride incubation times.

T(K)	Experimental parabolic Growth constant k (μm s $^{-0.5}$)	Boride incubation time $t_0^{Fe_2B}(T)$ (s)
1123	0.3729	1950
1173	0.6008	1950
1223	0.9392	1950
1273	1.300	1950

extrapolated at a value of $\frac{1}{T}=0$. The Q parameter is the activation energy which indicates the amount of energy (kJ mol^{-1}) required for the reaction to occur, and R is the ideal gas constant (R=8.314 J mol $^{-1}$.K^{-1}). The activation energy Q can be readily obtained from the slope of the curve relating $\ln(D_{Fe_2B})$ to the inverse of temperature. Hence, the expression of boron diffusion coefficient in the Fe_2B layers was obtained on the basis of Eq.(12) using the integral method for an upper boron content in Fe_2B equal to 9 wt.%.

Figure 8 shows the temperature dependence of boron diffusion coefficients in the Fe_2B layers according to Arrhenius relationship.

The expression of boron diffusion coefficient in the Fe_2B layer for AISI 4150 steel was obtained, using a linear fitting, in the temperature range of 1123-1273 K with a coefficient of determination close to unity:

$$D_{Fe_2B}=3.7\times10^{-3}\exp\left(\frac{-199.74 kJmol^{-1}}{RT}\right) \quad \ldots (16)$$

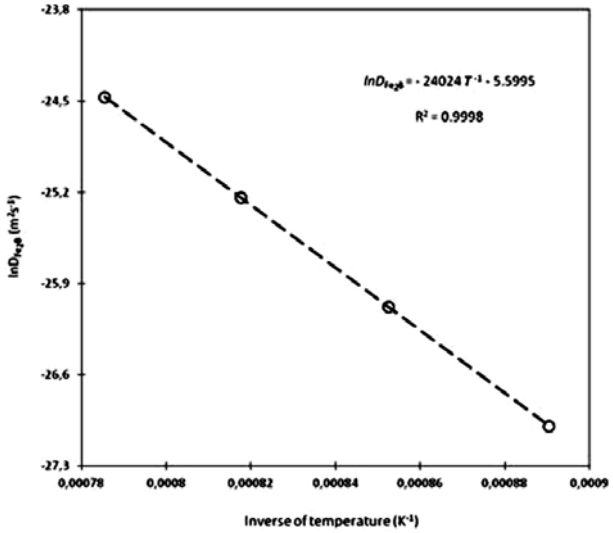

Fig. 8 — Arrhenius relationship for the boron diffusion coefficient through the Fe_2B layer.

where R = 8.314 J mol^{-1} K^{-1} and T the absolute temperature in Kelvin.

Different diffusion models were used to estimate the values of activation energy for boron diffusion in AISI 4150 steel for an upper boron content equal to 9 wt.%. Table 2 displays the values of boron activation energies estimated from three different models together with the expressions used to estimate the Fe_2B layer thickness. The obtained values of activation energy for boron diffusion are very comparable for all models in spite of difference in the mathematical formulation of each diffusion problem. All these models considered the principle of mass conservation at the (Fe_2B/ substrate) interface under certain assumptions. The Eq.s displayed in Table 2 can be used as a simple tool to predict the boride layer thickness for given boriding conditions.

Table 3 shows a comparison between the values of activation energy for boron diffusion in AISI 4150 steel and the values found in the literature for some borided materials [6,19, 26, 27, 60-68]. It is seen that the reported values of activation energy for boron diffusion in some steels and Armco iron depend on various factors such as: (the boriding method, the method of calculation, the nature of boriding agent, the temperature range considered, the mechanism of boron diffusion and the chemical composition of substrate). The values of activation energy for boron diffusion in AISI 4150 steel (193.45-199.74 kJ mol^{-1})

obtained from different diffusion models were interpreted as the amount of energy for the movement of boron atoms in the easiest path direction [001]

Table 2 — Values of boron activation energies estimated from three different models and together with the expressions used to estimate the Fe_2B layer thickness.

D_0 (m^2 s^{-1})	Activation energy Q ($kJmol^{-1}$)	Eq.s for estimating the Fe_2B layer thickness	References
3.76×10^{-3}	193.45	$u(t)=\sqrt{\frac{8D_{Fe_2B}(C_{up}^{Fe_2B}-C_{low}^{Fe_2B})t}{\ln(\frac{t}{t_0^{Fe_2B}})(C_{up}^{Fe_2B}+C_{low}^{Fe_2B}-2C_0)}}$	25
5.80×10^{-3}	198.43	$u(t)=2\varepsilon\sqrt{D_{Fe_2B}t}$ with ε = 0.0976	24
3.70×10^{-3}	199.74	$u(t)=\sqrt{\frac{D_{Fe_2B}[t-t_0^{Fe_2B})]}{\eta}}$ with η=13.3175	Present work

Table 3 — Comparison of activation energy for boron diffusion in AISI 4150 steel with other borided materials by using different boriding methods.

Material	Boriding method	Temperature range (K)	Boron activation energy ($kJ\ mol^{-1}$)	References
AISI 304 steel	Salt bath	1073-1223	253.33 (FeB+Fe_2B)	60
AISI H13 Steel	Salt bath	1073-1223	244.37 (FeB+Fe_2B)	60
AISI 4140 Steel	Salt bath	1123-1223	215.0 (FeB+Fe_2B)	61
AISI 1018 Steel	Electrochemical	1123-1273	172.75± 8.6 (FeB+Fe_2B)	62
Manganese Steel	Electrochemical	1023-1173	173.97 (FeB+Fe_2B)	63
Armco iron	Gaseous	1073-1273	78.03 (FeB) 120.65 (Fe_2B)	64
Armco iron	Paste	1123-1273	151.0 (Fe_2B)	65
AISI 4140 Steel	Paste	1123-1273	168.5 (Fe_2B)	27
AISI 8620 Steel	Plasma paste boriding	973-1073	124.7-138.5 (FeB+Fe_2B)	66
AISI 440C Steel	Plasma paste boriding	973-1073	134.62 (FeB+Fe_2B)	19
Armco iron	Powder	1123-1273	157.5 (Fe_2B)	26
AISI 51100 Steel	Powder	1123-1223	106.0 (Fe_2B)	67
AISI P20 Steel	Powder	1123-1223	(FeB+Fe_2B) 256.4 (in conventional furnace) and213.935 (in microwave furnace)	68
AISI 1045Steel	Powder	1123-1273	180.0 (Fe_2B)	6
AISI 4150 Steel	Powder	1123-1273	193.45-199.74 (Fe_2B)	Present work

along the boride layer that minimizes the growth stresses[55]. This value of energy is necessary to overcome the energetic barrier to allow the boron diffusion inside the metallic substrate. Thus, the diffusion phenomenon of boron atoms can occur along the grains boundaries and also in volume to form the Fe_2B layer on the steel's substrate. As a main remark, the differences seen in the values of activation energy for boron diffusion (see Table 3) in some borided steels indicate that the rate-determining steps in powder and paste boriding deviate from that for plasma paste boriding and that for gas boriding [19, 26,64].

4.5 Experimental validation of the diffusion models

The diffusion models were validated experimentally by comparing the experimental value of Fe_2B layer thickness with the predicted values. Figure 9 shows the optical micrograph of cross-section of the sample borided at 1253 K for 2.5 h.

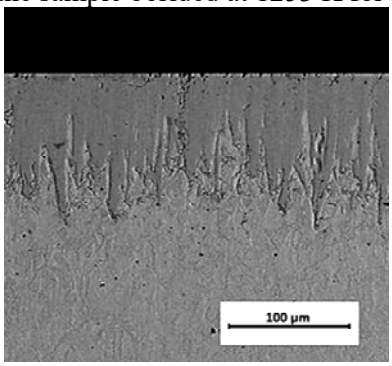

Fig. 9 — Optical micrograph of Fe_2B layer formed on the AISI 4150 steel at 1253 K for 2.5 h.

Table 4 shows a comparison between the experimental value of Fe_2B layer thickness (obtained

Table 4 — Comparison between the experimental value of Fe_2B layer thickness (obtained at 1253 K for 2.5 h) and the predicted values using three different models for an upper boron content in the Fe_2B phase equal to 9 wt.%.

Boriding conditions	Experimental Fe_2B layer thickness (μm)	Simulated Fe_2B layer thickness (μm) By the numerical model [30]	Simulated Fe_2B layer thickness (μm) by the diffusion model [25]	Simulated Fe_2B layer thickness(μm) by the diffusion model [24]	Simulated Fe_2B layer thickness(μm) by the integral method
1253 K for 2.5 h	95.94± 15.89	102.0	103.04	103.06	96.04

at 1253 K for 2.5 h) and the predicted values using different diffusion models for an upper boron content in the Fe_2B phase equal to 9 wt.%. It is seen that the predicted values of boride layers' thicknesses agree in a satisfactory manner with the experimental value**,** for an upper boron content in the Fe_2B phase equal to 9 wt.%.

Table 5 — Diffusivities of boron in Fe_2B and austenite used as input in the numerical model [30].

Parameters	Expression
D_{Fe_2B} ($m^2\ s^{-1}$)	$9.28\times10^{-3}\exp(-\frac{198.43kJ}{RT})$
D_{γ} ($m^2\ s^{-1}$)	$4.4\times10^{-8}\exp(-\frac{81.53kJ}{RT})$ With R=8.314 J mol^{-1} K^{-1}

In the numerical model suggested by Kouba *et al.*[30], the boron flux at the material surface was found to be equal to 1.6×10^{-4} mol s^{-1} m^2 after many numerical tests. This adjustable parameter for the numerical model allowed us to find a value of the boride incubation time very close to 1950 s, which is required for the formation of a compact layer of Fe_2B. The diffusivities of boron in Fe_2B and austenite used for predicting the Fe_2B layer thickness obtained at 1253 K for 2.5 h are given in Table 5. The expressions of Fe_2B layer thickness listed in Table 2 are depending on the boriding parameters (the treatment time and the boriding temperature). They can be used as a tool to predict the optimum value of boride layer thickness according to the industrial application of this kind of borided steel.

Acknowledgements

The work described in this paper was supported by a grant of PRODEP and CONACyT México. Likewise, FCS acknowledge funding from the Physics and Mathematics Department and the Research Division within UIA. Authors are grateful with the Microscopy Lab at UIA.

5 Conclusions

In this study, the growth kinetics of Fe_2B layers formed on AISI 4150 steel was investigated by use of different approaches in the temperature range of 1223-1273 K for periods of 2-8 h.

(i) A compact Fe_2B layer was formed for all boriding conditions at the surface of AISI 4150 steel. Its existence was confirmed by XRD analysis.

(ii) The (Fe_2B/substrate) interface had a tooth shaped morphology with a boride layer thickness ranged from 27.29 ±3.21 to 213.01 ± 24.3 μm. The growth kinetics of boride layers obeyed the parabolic growth law with an occurrence of a constant boride incubation time.

(iii) The interfacial cohesion of the Fe_2B layers on AISI 4150 steel (obtained at 1173 K for 2 and 8 h) were respectively related to HF3 and HF2 categories according to the VDI 3198 norm. As a result, the borided sample at 1173 K for 8 h showed a best cohesive quality.

(iv) The values of activation energy for boron diffusion in AISI 4150 steel ranged from 193.45 to 199.74 $kJmol^{-1}$. These estimated values depend on the diffusion models used.

(v) A good agreement was then observed between the experimental value of Fe_2B layer thickness (obtained at 1253 K for 2.5 h) and the predicted values of Fe_2B layer thickness using different diffusion models.

List of symbols

u(t) is the boride layer thickness (μm).

a(t) and b(t) are the time-dependent parameters

k is the parabolic growth constant of the Fe_2B layer ($\mu m s^{-0.5}$).

t is the treatment time (s).

$t_0^{Fe_2B}(T)$ is the boride incubation time (s).

$C_{up}^{Fe_2B}$ represents the upper limit of boron content in Fe_2B (=9 wt.%).

$C_{low}^{Fe_2B}$ is the lower limit of boron content in Fe_2B (=8.83wt.%).

C_{ads} is the adsorbed boron concentration in the boride layer (wt..%).

C_0 is the boron solubility in the matrix (≈ 0 wt.%).

$C_{Fe_2B}[x,t]$ is the boron concentration profile in the

Fe_2B layer (wt.%).

D_{Fe_2B} represents the diffusion coefficient of boron in the Fe_2B phase ($m^2\ s^{-1}$).

Q is the activation energy for boron diffusion ($kJmol^{-1}$)

References

1 Sinha A K, Boriding, *J Heat Treat*, 4 (1991) 437.
2 Medvedovski, E, Adv Eng Mater, 18 (2015)11.
3 Campos I, Palomar M, Amador A, Ganem R, & Martinez J, Surf Coat Technol, 201 (2006) 2438.
4 Béjar M A, & Moreno E, J Mater Process Technol, 173 (2006) 352.
5 Sen U, & Sen S, *Mater Character*, 50 (2003) 261.
6 Zuno-Silva J, Ortiz-Domínguez M, Keddam M, Elias-Espinosa M, Damián-Mejía O, Cardoso-Legorreta E & Abreu-Quijano M, *J Min Metall Sect B-Metall*, 50 (2014) 101.
7 Ulutan M, Yildirim M M, Celik O N & Buytoz S, *Tribol Lett,* 38 (2010) 231.
8 Calik A, Ucar N, Karakas M S & Tanis H, *High Temp Mater Proc*, 38 (2019) 342.
9 Türkmen İ, & Yalamaç E, *J Alloys Compounds*, 744 (2018) 658.
10 Gunes I, & Kanat S, *Protec Met Phys Chem Surf*, 51 (2015) 842.
11 Campos I, Ramırez G, Figueroa U, Martinez J & Morales O, *Appl Surf Sci,* 253 (2007) 3469.
12 Ortiz-Domínguez M, Campos-Silva I, Hernández-Sánchez E, Nava-Sánchez J L, Martínez-Trinidad J, Jiménez-Reyes M Y & Damián-Mejía O, *Int J Mater Res*, 102 (2011) 429.
13 Simonenko A N, Shestakov V A & Poboinya V N, *Met Sci Heat Treat*, 24 (1982) 360.
14 Smol'nikov E A, & Sarmanova L M, *Met Sci Heat Treat*, 24 (1982) 785.
15 Segers L, Fontana A, & Winand R, *Electrochimica Acta*, 36 (1991) 41.
16 Kulka M, Makuch N & Piasecki A, *Surf Coat Technol,* 325 (2017) 515.
17 Kulka M, Makuch N, Pertek A, & Piasecki A, *Mater Character*, 72 (2012) 59.
18 Küper A, Qiao X, Stock H R, & Mayr P, *Surf Coat Technol*, 130 (2000) 87.
19 Keddam M, Chegroune R, Kulka M, Panfil D, Ulker S & Taktak S, *Trans Indian Inst Met,* 70 (2017) 1377.
20 Yang H P, Wu X C, Min Y A, Wu T R, & Gui J Z, *Surf Coat Technol*, 228 (2013) 229.
21 Larisch B, Brusky U, & Spies H J, *Surf Coat Technol*, 116-119 (1999) 205.
22 *Sahin S & C Meric C,* Mater Res Bulletin, *37 (2002) 971.*
23 *Jain V & Sundararajan G,* Surf Coat Technol, *149 (2002) 21.*
24 Elias-Espinosa M, Ortiz-Domínguez M, Keddam M, Gómez-Vargas O A, Arenas-Flores A, Barrientos-Hernández F R, West Anthony R & Sinclair Derek C*, Surf Eng,* 31 (2015) 588.
25 Ortiz-Domínguez M, Flores-Rentería M A, Keddam M, Elias-Espinosa M, Damián-Mejía O, Aldana-González J I, Zuno-Silva J, Medina-Moreno S A & González-Reyes J G, *Mater Technol*, 48 (2014) 905.
26 Elias-Espinosa M, Ortiz-Domínguez M, Keddam M, Flores-Rentería M A, Damián-Mejía O, Zuno-Silva J, Hernández-Ávila J, Cardoso-Legorreta E & Arenas-Flores A, *J Mater Eng Perform*, 23 (2014) 2943.
27 Nait Abdellah Z, Keddam M & Elias A, *Int J Mater Res,* 104 (2013) 260.
28 Nait Abdellah Z, Keddam M, Chegroune R, Bouarour B, Lillia H & Elias A, *Matériaux et Techniques*, 100 (2012) 581.
29 Keddam M, Ortiz-Dominguez M, Elias-Espinosa M, Arenas-flores A, Zuno-Silva J, Zamarripa–Zepeda D & Gomez-Vargas O A, *Metall Mater Transac A*, 49 (2018) 1895.
30 Kouba R, Keddam M & Kulka M, *Surf Eng*, 31 (2015) 563.
31 Campos I, Islas M, Gonzalez E, Ponce P & Ramírez G, *Surf Coat Technol*, 201 (2006) 2717.
32 Campos I, Bautista O, Ramírez G, Islas M, De La Parra J & Zúñiga L, *Appl Surf Sci*, 243 (2005) 429.
33 Perrusquia N L, Doñu Ruiz M A, Oliva E Y V, & Suarez V C, *MRS Proc*, 1481 (2012) 105.
34 Ramdan R D, Takaki T & Tomita Y, *Mater Transac*, 49 (2008) 2625.
35 Mebarek B, Madouri D, Zanoun A & Belaidi A, *Matériaux Techniques*, 103 (2015) 703.
36 Mebarek B, Benguelloula A, & Zanoun A, *Mater Res*, 21 (2018) e20170647.
37 Mebarek B, Zanoun A & Rais A, *Metall Res Technol*, 104 (2016) 113.
38 Mendoza C I V, Mendoza J L R, Galván V I, Hodgkins R P, Valdivieso A L, Palacios L L S, & Junquera V I, *Int J Surf Sci Eng*, 8 (2014) 71.
39 Leon Cazares F, Jimenez Ceniceros A, Oseguera Pena J & Castillo Arangurena F, *Revista Mexicana de Fısica*, 60 (2014) 257.
40 Ernesto M H, Jose A O, Antonio J, Ruben D S, Raul M, Francisco C & Joaquin E O, *Scien Res Essays*, 11 (2016) 135.
41 Brakman C M, Gommers A W J & Mittemeijer E J, *J Mater Res,* 4 (1989) 1354.
42 Yu L G, Chen X J, Khor K A & Sundararajan G, *Acta Materialia,* 53 (2005) 2361.
43 Krukovich M G, Prusakov B A & Sizov I G, The Components and Phases of Systems 'Boron-Iron' and 'Boron-Carbon-Iron', Chapter Plasticity of Boronized Layers, (Springer: Materials Science), 237 (2016) 13.
44 Okamoto H, *J Phase Equilibria Diffusion*, 25 (2004) 297.
45 Busby P E, & Wells C, *JOM*, 6 (1954) 972.
46 Okamoto H, *J Phase Equilibria Diffusion*, 25 (2004) 297.
47 Goodman T R, *Adv Heat Transfer*, 1 (1964) 51.
48 Campos-Silva I, Bravo-Bárcenas D, Meneses-Amador A, Ortiz-Dominguez M, Cimenoglu H, Figueroa-López U & Tadeo-Rosas R, *Surf Coat Technol*, 237 (2013) 402.
49 Ortiz Domínguez M, *Contribución de la Modelación Matemática en el Tratamiento Termoquímico de Borurización*, Ph.D. thesis, National Polytechnic Institute of Mexico, 2013.
50 Campos-Silva I, Ortiz-Domínguez M, Bravo-Bárcenas O, Doñu-Ruiz M A, Bravo-Bárcenas D, Tapia-Quintero C & Jiménez-Reyes M Y, *Surf Coat Technol*, 205 (2010) 403.
51 Campos-Silva I, Ortiz-Domínguez M, Tapia-Quintero C, Rodríguez-Castro G, Jiménez-Reyes M Y, & Chávez-Gutiérrez E, *J Mater Eng Perform*, 21 (2011) 1714.
52 Vidakis N, Antoniadis A & Bilalis N, *J Mater Process Technol* , 143-144 (2003) 481.
53 Taktak S, *Mater Des*, 28 (2007) 1836.

54 Rodríguez-Castro G A, Jiménez-Tinoco L F, Méndez-Méndez J V, Arzate-Vázquez I, Meneses-Amador A, Martínez-Gutiérrez H & Campos-Silva I, *Mater Res*, 18 (2015) 1346.
55 Taktak S & Tasgetiren S, *J Mater Eng Perform*, 15 (2006) 570.
56 Martini C, Palombarini G & Carbucicchio M, *J Mater Sci*, 39 (2004) 933.
57 Carbucicchio M, Meazza G & Palombarini G, *J Mater Sci*, 17 (1982) 3123.
58 Dukarevich I S, Mozharov M V & A S Shigarev A S, *Met Sci Heat Treat*, 15 (1973) 160.
59 Kartal G, Timur S, Sista V, Eryilmaz O L & Erdemir A, *Surf Coat Technol*, 206 (2011) 2005.
60 Taktak S, *J Mater Sci*, 41 (2006) 7590.
61 Sen S, Sen U & Bindal C, *Vacuum*, 77 (2005) 195.
62 *Kartal G, Eryilmaz O L, Krumdick G, Erdemir A & Timur S,* Appl Surf Sci*, 257 (2011) 6928.*
63 *Matiašovský K, Chrenková-Paučírová M, Fellner P & Makyta M,* Surf Coat Technol*, 35 (1988) 133.*
64 Keddam M, Kulka M, Makuch N, Pertek A & Małdziński L, *Appl Surf Sci,* 298 (2014) 155.
65 *Campos I, Oseguera J, Figueroa U, Garcia J A, Bautista O & Kelemenis G,* Mater Sci Eng A*, 352 (2003) 261.*
66 Gunes I, Taktak S, Bindal C, Yalcin Y, Ulker S & Kayali Y, *Sadhana*, 38 (2013) 513.
67 Ipek M, Celebi Efe G, Ozbek I, Zeytin S & Bindal C, *J Mater Eng Perform*, 21 (2012) 733.
68 Kayali Y, *Vacuum,* 121 (2015) 129.